Composites: Part A 151 (2021) 106660

Contents lists available at ScienceDirect

Composites Part A

journal homepage: www.elsevier.com/locate/compositesa

Evaluation of interfacial, dispersion, and thermal properties of carbon Fiber/ABC added epoxy composites manufactured by VARTM and RFI methods

Jong-Hyun Kim [a,b], Pyeong-Su Shin [a,b], Dong-Jun Kwon [b], K. Lawrence DeVries [c], Joung-Man Park [a,b,c,*]

[a] Department of Materials Engineering and Convergence Technology, Gyeongsang National University, Jinju, 52828, Republic of Korea
[b] Research Institute for Green Energy Convergence Technology (RIGET), Gyeongsang National University, Jinju, 52828 Republic of Korea
[c] Department of Mechanical Engineering, The University of Utah, Salt Lake City, UT, 84112, USA

ARTICLE INFO

Keywords:
Activated bamboo charcoal (ABC)
Dispersion evaluation
Thermal properties
Interfacial properties

ABSTRACT

This study investigated the effect of activated bamboo charcoal (ABC) for improving thermal and interfacial properties in carbon fiber (CF) reinforced epoxy. Two manufacturing methods, vacuum assisted resin transfer molding process (VARTM) and resin film injection (RFI) processes were compared. Tensile and flexure properties of ABC added epoxy (EP), with different ABC weight fractions were evaluated. Comparative dispersion of ABC was evaluated using two dimensional (2D) electrical resistance (ER) and weight mappings for two manufacturing processes. Specimen using RFI process exhibited more stable ER than VARTM. Both interlaminar and interfacial shear strengths (ILSS & IFSS) of the CF/ABC-EP composites were consistent. RFI process was better suited for manufacturing ABC added fiber reinforced composite than VARTM process. For both at initial case and after 30 days thermal degradation, 10 wt% ABC added CF/EP composite was determined for maximum mechanical, interfacial and thermal properties due to suitably-dispersed ABC with stress transfer uniformly.

1. Introduction

Activated bamboo charcoal (ABC), a by–product of organic waste pyrolysis, is a renewable material which had been extensively employed in agriculture and environmental management as a low cost carbon sequester and a natural adsorbent [1,2]. ABC has the potential of use as the reinforcement of composites to improve mechanical and flammability/thermal properties. When ABC was produced at high temperature (>500 °C), the numerous pores on ABC surface exhibited. The ABC had stabled honeycomb-like carbonaceous structure with a high surface area and the advantage of ABC could be employed in other areas as well, thereby diversifying its potential applications [3–5]. Mechanical bonding/interlocking occurred between the ABC and the polymer matrix and potentially mechanical properties of the composite were enhanced [6–10]. In addition, the high thermal stability of ABC might enhance heat-resistance properties of composites [11,12].

Many researchers have tried to broaden the application fields of fiber reinforced composites through the use of nanoparticles. This produced multiscale composites with enhanced mechanical, electrical, thermal properties [13,14]. In traditional manufacturing methods of composites, nanoparticle was firstly being "pre-dispersed" in the resin. Nanoparticle dispersed resin subsequently was injected in the microscale fiber reinforcements during composite fabrication. [15,16]. However, this method had a critical defect in that the nanoparticles in resin were filtered by the fiber mats resulting in relatively poor dispersion of the nanoparticles [17,18]. Inhomogeneous filler content and thus defective composite parts with non-uniform properties occurred by filtration of the nanoparticles. In the most severe conditions, impregnation of nanoparticle added polymer resin was difficult or hindered in case of high-fiber content fabrics or high filler contents [19,20].

A resin film infusion (RFI) method was proposed to enrich enough amounts of nano-filler on the composite surface while maintaining a uniform distribution in-plane [21]. It has been developed as a cost-effective technique for the fabrication of complex shaped parts resolving several critical concerns of conventional liquid composite molding methods. RFI also ensures near zero void fractions because of better compaction and local flow of the polymer resin [22,23]. RFI provided for better dispersion of the nanoparticles in the matrix for a

* Corresponding author.
E-mail address: jmpark@gnu.ac.kr (J.-M. Park).

https://doi.org/10.1016/j.compositesa.2021.106660
Received 28 January 2021; Received in revised form 18 September 2021; Accepted 20 September 2021
Available online 24 September 2021

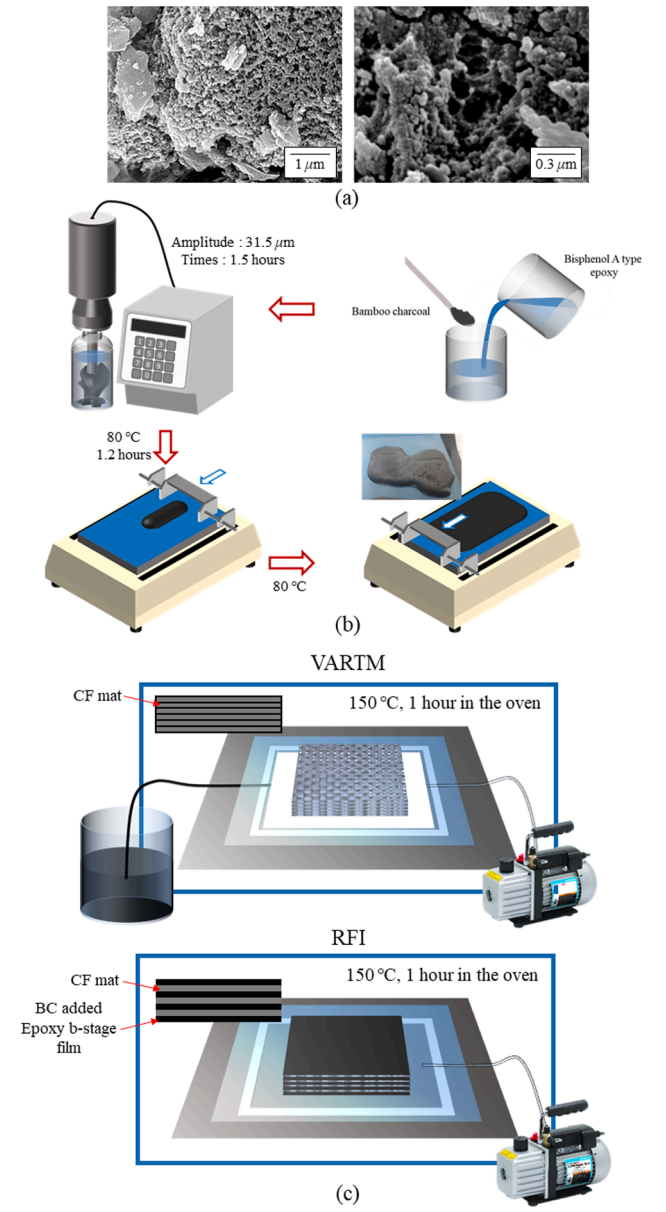

Fig. 1. Schematic arrangement of manufacturing process of CF/ABC-EP composite: (a) ABC-EP b-stage film; and (b) CF/ABC-EP composite manufacturing process.

cost-effective, bulk modification of the polymer matrix. This process was a more scalable manufacturing approach for multiscale, hybrid composites [24].

In this paper, the effect of ABC for improving thermal and interfacial properties was evaluated in CFRP for different ABC weight fractions. The ABC dispersion was compared for the different manufacturing processes using tensile test and electrical property measurements. Mechanical properties of the ABC added epoxy matrix, with different ABC weight fractions, were evaluated using tensile and flexural tests. TGA was used to evaluate the thermal properties of ABC-EP matrix with different ABC weight fractions. Interfacial properties of CF/ABC-EP composites were evaluated by interlaminar shear strength (ILSS) and interfacial shears strength (IFSS) *via* short beam shear and microdroplet pull-out tests. The conditions were set up with different ABC weight fraction and thermal degradation time. The results were used to evaluate the relationship between interfacial and mechanical properties and to obtain the optimal ABC weight fraction.

2. Experimental

2.1. Materials

T-700 grade woven type CF fabric (Toray Inc., Japan) was used as the composite reinforcement. Activated bamboo charcoal (ABC) powder (Samchun Chem., Korea) was used as the epoxy (EP) matrix reinforcement and to improve thermal properties. The surface area of ABC was measured using BET equipment (3Flex, Micrometrics Co., U.S.A.) at Center for Research Facilities in our University. The pyrolysis of ABC was performed at 500 ℃ to remove residual biomass and water, followed further by the high temperature activation at 900 ℃. In Fig. 1(a), the ABC surface area of ABC was 750 m^2/g after pyrolysis process. Many pores with different sizes were observed in ABC surface. Bisphenol-A type epoxy (YD-128), Kukdo Chem., Korea) and anhydride type hardener (KBH-1089, Kukdo Chem., Korea) were used as the matrix. The plate specimens of CF/ABC-EP composite were cut by a diamond cutter (MBS 220E, Proxxon Co., Ltd., Japan) to produce the short beam test specimens.

2.2. Methodologies

2.2.1. Dispersion of ABC particle with different manufacturing process of CF/ABC-EP composite

Fig. 1(b) shows a schematic arrangement of the manufacturing process of ABC-EP b-stage film in the manufacture of CF/ABC-EP composites. ABC was dispersed in epoxy resin using ultrasonication equipment (VC-505, Sonics & Materials, U.S.A.) at 31.5 μm of wave amplitude for 1.5 h. After dispersion, the ABC-EP resin was heated to 80 ℃ for 1.2 h using an oven (OF-22GW, Jeio Tech Co., Ltd., Korea) to increase viscosity and molecular weight of the epoxy resin. The epoxy b-stage film was formed using a bar coater at 50 ℃ to 1 mm thickness to maintain the viscosity of the epoxy resin and to cool it down to room temperature. The CF/ABC-EP composite was manufactured using the RFI process to improve dispersion of the ABC particles.

Fig. 1(c) shows a schematic arrangement for manufacturing of the CF/ABC-EP composites. In the VARTM process, the ABC particles were more poorly dispersed than in the RFI process because the ABC particles were filtered by the fibers. In the RFI process, however, the ABC particles were dispersed in the epoxy b-stage film before the CF/ABC-EP composite was manufactured. The ABC-EP b-stage films and woven type CF mats were laminated alternately. After vacuum bagging, the ABC-EP b-stage films and CF mats were cured at 150 °C in vacuum using a drying oven and vacuum pump (GLD-137AA, Ulvac Inc., Japan).

2.2.2. Mechanical and thermal properties of ABC-EP matrixes with different ABC weight fractions

The mechanical properties of ABC-EP matrixes, with different ABC fractions, were determined using tensile and flexural tests with different ABC weight fractions. The specimens were manufactured by pouring and curing the ABC added EP resin into poly(dimethylsiloxane) (KE-1300, ShinEtsu Chem., Japan) mold exhibiting the dog-bone and bar shapes. All of specimens were manufactured based on ASTM D638 and D790 and series of 5 tests were performed at 5 times using a UTM (H1K-S, Lloyd Instruments Ltd., U.K.). The Thermal behavior of ABC-EP matrixes was obtained using TGA (T50, TA Instruments, U.S.A.). The weight variation of sample was measured from 25 to 600 °C with increasing rate of 10 °C/minute under the flow of nitrogen. The relative thermal stability of the ABC-EP composite was determined by temperature at 5 and 10% weight loss, T_{d5} and T_{d10} [26,27].

2.2.3. Interfacial properties of CF/ABC-EP composite with different ABC weight fractions

The interfacial properties of CF/ABC-EP composites were evaluated using ILSS and IFSS. ILSS and IFSS specimens were thermos-degraded at 150 °C using a muffle furnace (MF-12G, Jeio Tech Co., Ltd., Korea) to

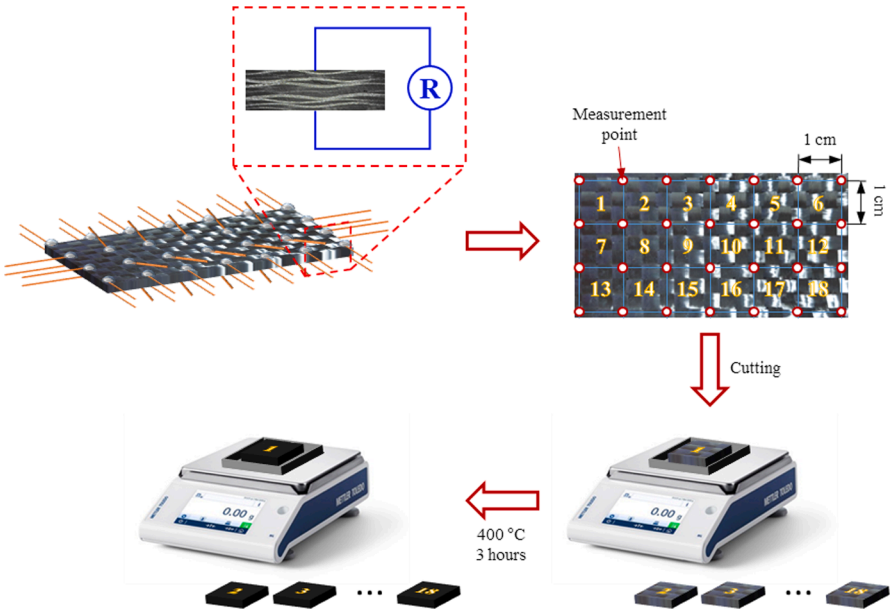

Fig. 2. Schematic arrangement for 2D-ER and weight mappings of CF/ABC-EP composite with different manufacturing processes.

evaluate the decrease in interfacial properties for different ABC weight fractions and thermal degradation times.

The ILSS of the CF/ABC-EP composites was obtained by the short beam shear test. The short beam test (ASTM D-2344) was used to evaluate the ILSS for specimens with the dimensions of 40 mm in length, 10 mm in width, and 2.3 mm in thickness. The ILSS was calculated using equation (2),

$$ILSS = \frac{3F}{4bd} \tag{2}$$

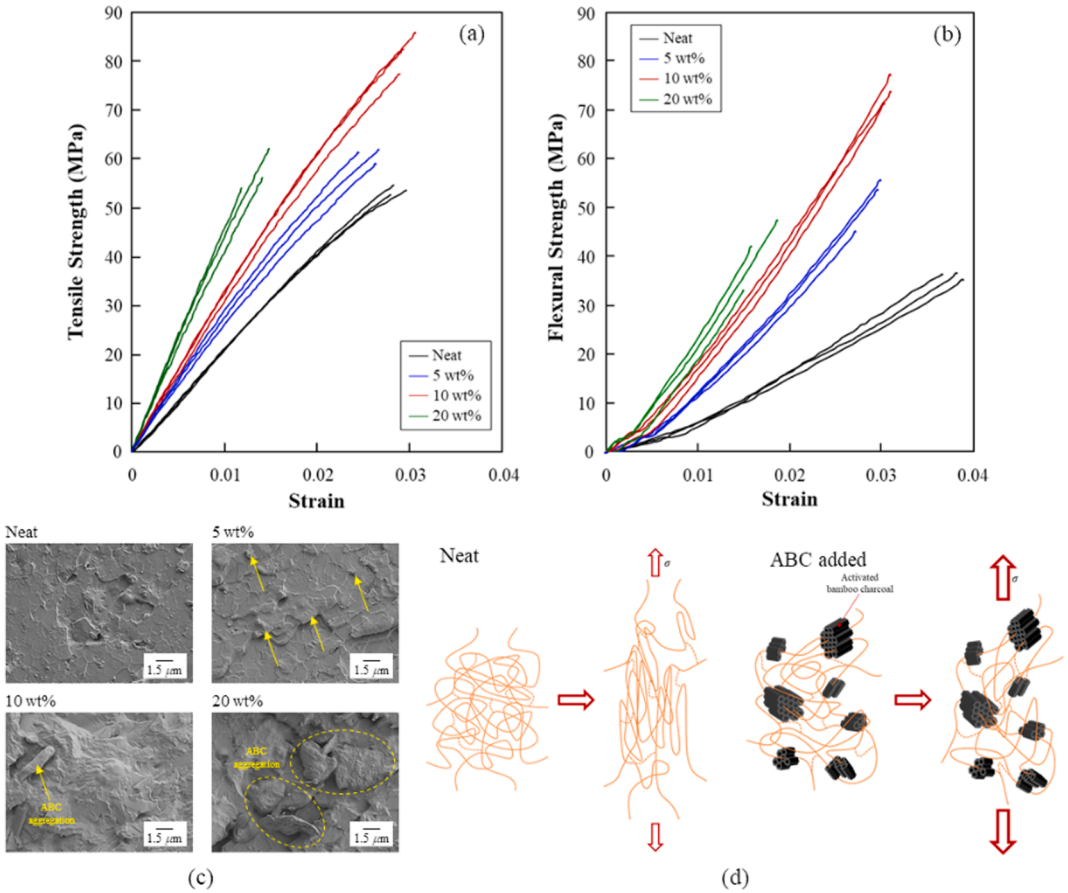

Fig. 3. Mechanical and thermal properties of epoxy matrix composites with different ABC weight fractions: (a) tensile strength; (b) flexural strength; (c) FE-SEM photo of fracture surface; and (d) schematic arrangement of ABC added EP composite during tensile strength.

where F is the failure force, while b and d are the thickness and width of the specimen. The experimental conditions for the ILSS test were set with a span of 20 mm at a flexural rate of 1 mm/minute. The results were given as an average using more than three tests.

The IFSS of the CF/ABC-EP composites was obtained *via* micro-droplet pull-out test. Single CFs were fixed in a steel frame and micro-droplets of neat and ABC-EP were dropped on each fiber. The microdroplets were cured at 80 °C for 1 h in an oven. The microdroplet was held using a special designed micrometer and the CF was pulled out. The IFSS was determined by equation (3)

$$IFSS = \frac{F}{\pi D_f L} \tag{3}$$

where F is the pull-out force, D_f is diameter of the CF, and L is the fiber embedded length in the ABC added EP. The gauge length was 5 mm and the pull out test speed was 0.5 mm/minute. This test was performed about 30 times with different-sized microdroplets from 50 to 190 μm range to determine the statistical trends of microdroplet slip and fiber fracture sections, and the IFSS was calculated at the cross point of two trend lines [28].

2.2.4. Evaluation of ABC dispersion in CF/EP composite with different manufacturing process

Fig. 2 shows the schematic arrangement of ER measurements relative to the z-axis of CF/ABC-EP composites. The 10 wt% ABC specimen was cut to a 30 mm in width and 50 mm in length. The ER in the direction of the z-axis was measured at 24 points using 2-probe ER measurements with the distance between the points set at 10 mm. Copper wires were attached to the CF/ABC-EP composites using silver paste (Elcoat P-100, CANS, Japan) and EP adhesive (AR-5, Huntsman Co., U.S.A.) to improve electrical conductivity between the copper wires and the CFRP. The EP adhesive was cured at 70 °C for 1 h in an oven. The ER variation was calculated using equation (1):

$$\mathrm{ERvariationratio}(\%) = \frac{(R - R_{average})}{R_{average}} \times 100 \tag{1}$$

where R is the ER at the points of measurement and $R_{average}$ is the average of the ER at the 24 points. After ER measurement, the specimens were cut to one cell size and the weight of specimens were measured using electrical scale (FX-200i, CAS Co., Ltd., Korea). The specimens were degraded at 400 ℃ for 3 h in a furnace (MF-12G, Jeio Tech Co., Ltd., Korea) to burn down the epoxy matrix. The weight of specimens was measured after burning out epoxy matrix sufficiently. The ER and weight variation data were visualized using a contour chart and this chart showed a 2D surface that connects a set of data points for the dispersion conditions for the CFRC. As on a contour map, the patterns on these charts indicate areas of similar value of ER [25].

The ABC dispersion in CF/EP composite was evaluated using tensile test and ER measurements with the different manufacturing processes. Composites that performed ER measurements, were cut for 20 specimens to 5 mm in width to compare tensile stress with different manufacturing process. The tensile test was performed using UTM and the tensile rate was set as 10 mm/minute.

3. Results and discussion

3.1. Mechanical and thermal properties of ABC-EP composites with different ABC weight fractions

Fig. 3 shows the tensile and flexural properties of ABC added EP nanocomposites with different ABC weight fractions. As shown in Fig. 3 (a), the tensile strength of ABC/EP composites increased for the different ABC weight fractions. The tensile strength increased up to 10 wt% ABC addition. However, over 10 wt% ABC addition, the tensile strength decreased while tensile modulus increased as the ABC weight fraction

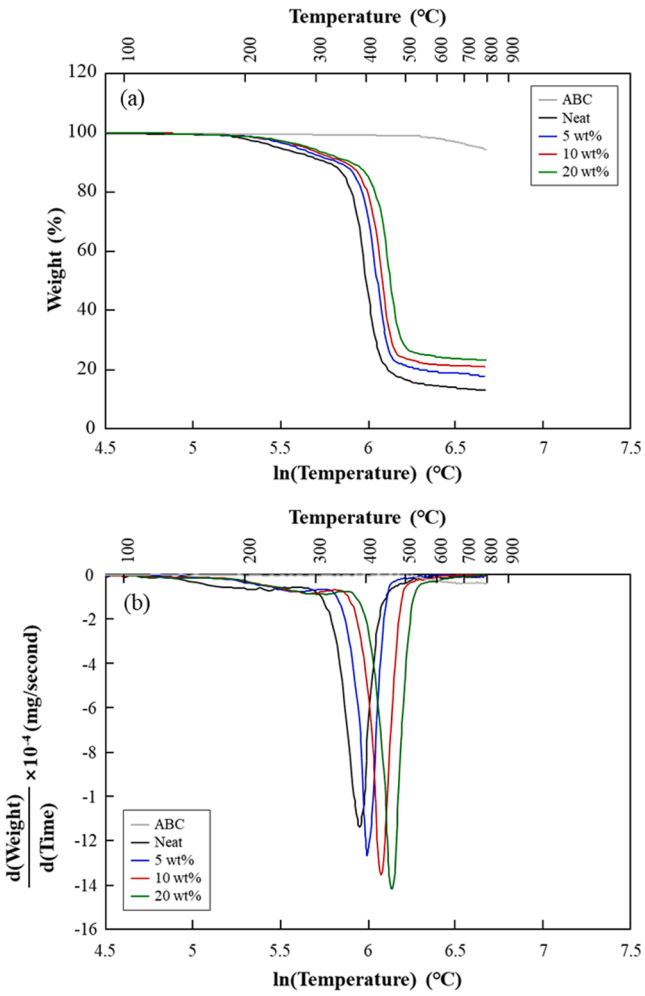

Fig. 4. Thermal properties of epoxy matrix with different ABC weight fractions: (a) TGA; and (b) DTG.

increased. In Fig. 3 (b), the flexural strength and modulus exhibited similar trends to that of the tensile strength and modulus.

In FE-SEM photographs as shown in Fig. 3(c), ABC particles were observed along with a number of pores formed on the ABC particle surfaces in which affected the surface area of ABC particles, the increasing interlocking with the EP matrix [29,30]. The mechanical properties of ABC/EP composite increased with increasing the interfacial area between ABC and EP. However, over 10 wt% ABC addition, the ABC crack propagation was apparently affected through by the ABC cohesion area.

In Fig. 3(d), the schematic arrangement with ABC addition exhibited with adding ABC. The ABC added EP matrix showed both higher mechanical strength and modulus than the neat epoxy matrix. In the tensile test, the neat EP chain was stretched unrestrictedly, whereas the EP chain mobility in ABC added EP was restricted more due to the steric

Table 1
The temperature of the 5 and 10% weight loss of epoxy matrix with different ABC weight fractions.

Type (wt%)	T_{d5} [1] (°C)	T_{d10} [2] (°C)
0	261	343
5	288	369
10	304	384
20	310	396

[1] Temperature at weight loss at 5 %
[2] Temperature at weight loss at 10 %

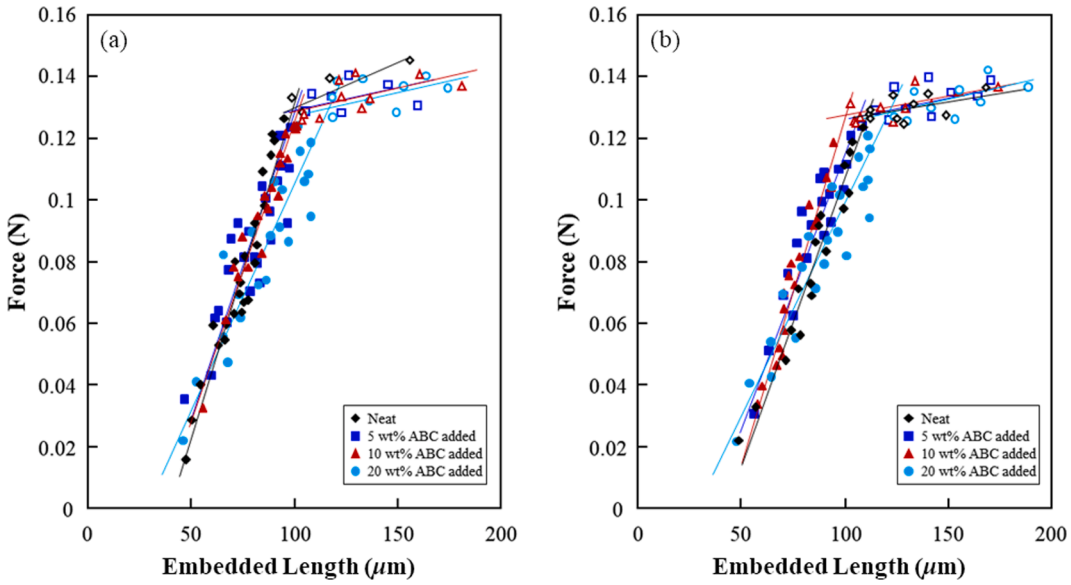

Fig. 5. IFSS of CF/ABC-EP composites with different ABC weight fractions and degradation times: (a) the initial; and (b) after 30 days.

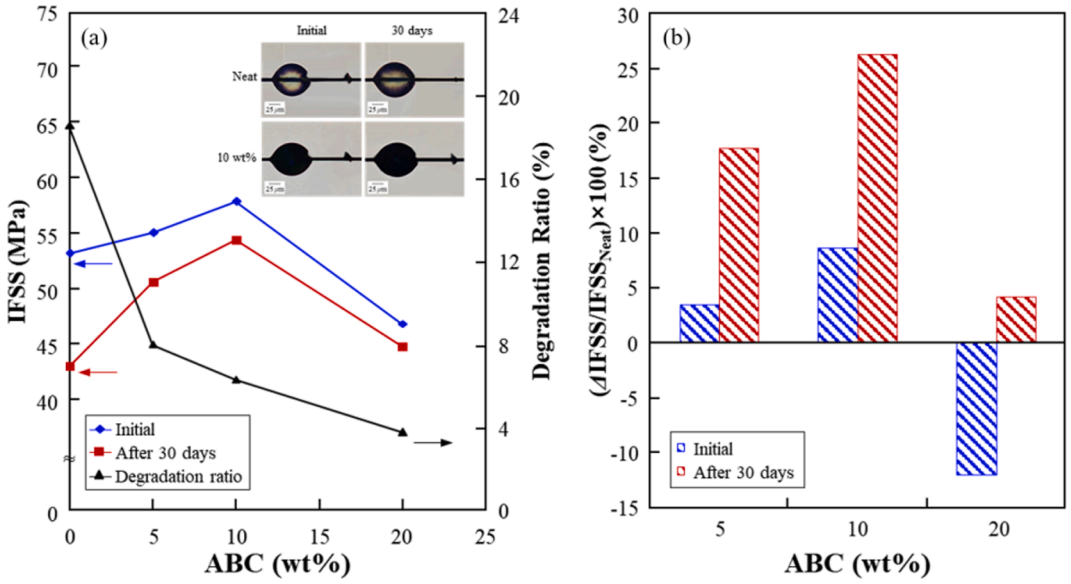

Fig. 6. Interfacial properties of microdropelt pull-out test with different ABC weight fractions: (a) IFSS; and (b) difference of IFSS *versus* elapsing time of thermal degradation.

hindrance by the rigid micro-pores in ABC. It resulted in increasing both tensile strength and modulus. In the case of flexural loading, more stress resistance by steric hindrance due to the addition of the reinforcement of ABC for both upon compression on upper side and for tensile stress on the bottom side. It resulted in increasing both flexural strength and modulus.

Table 2
IFSS and degradation ratio with different ABC weight fractions and degradation times.

ABC weight fraction (wt%)	IFSS (MPa)		Degradation ratio(%)
	Initial	After 30 days	
0	53.2	43.3	18.6
5	55.1	50.7	8.1
10	57.8	54.1	6.4
20	46.8	45.0	3.8

Fig. 4(a) and Table 1 show thermal properties using TGA on EP matrix composites with different ABC weight fractions. The weight loss was initially rather gradual followed by a much more rapid decrease at around 400 °C. Increase in the weight fraction of ABC in the composites resulted in somewhat less weight loss at each TGA temperature, as illustrated in Fig. 5 and more quantitatively in Table 1. The DTG graphs exhibited in Fig. 4(b) using TGA data of ABC added EP matrix. The initial decreasing behavior of ABC was shown approximately at 500 ℃, and it could be due to residual materials inside ABC. The neat EP matrix was degraded initially starting from 190 °C

3.2. IFSS of CF/ABC-EP composites with different ABC weight fractions

Fig. 5 shows plots of microdroplet pull out tests for different ABC weight fractions, both the initial and after 30 days. As shown in Fig. 5(a), the slope of the line for ABC-EP microdroplet slipping on the CF surface (closed circle) increased slightly as the ABC weight fraction increased.

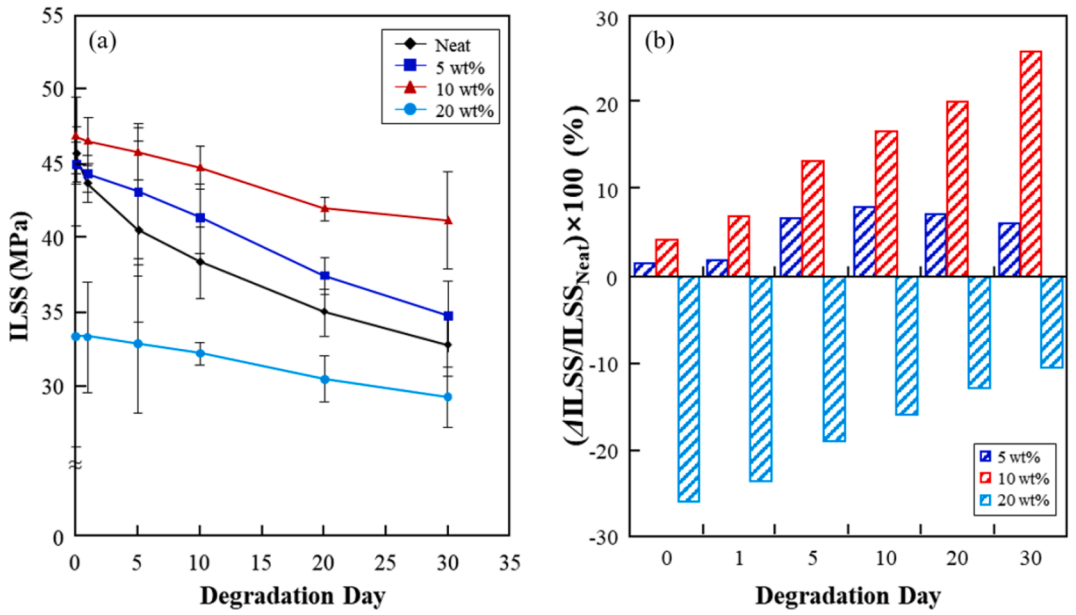

Fig. 7. Interfacial property of short beam test of CF/ABC-EP composites with different ABC weight fractions: (a) ILSS; and (b) the difference in ILSS *versus* the elapsing time of thermal degradation.

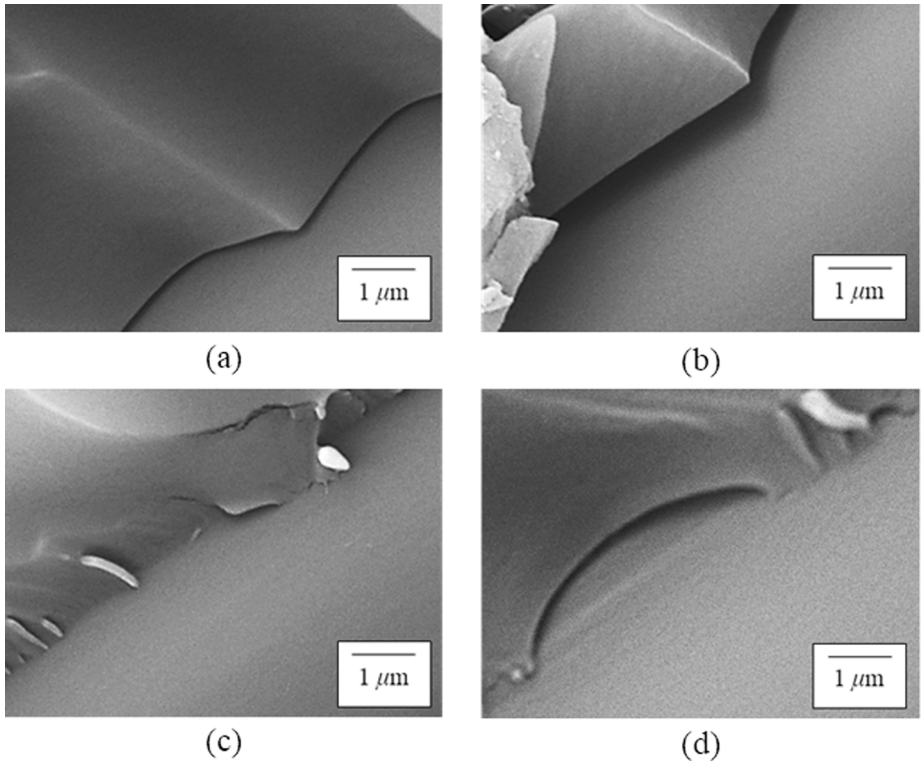

Fig. 8. FE-SEM photos of interface between CF and EP: (a) neat/initial; (b) neat/degraded; (c) ABC added/initial; and (d) ABC added/degraded.

For over 10 wt% ABC addition, the slope of the line for microdroplet slipping decreased appreciably. This indicates that, for the same size microdroplets, the load needed to cause slip to increase as the ABC weight fraction increased up to 10 wt%. After 30 days of thermal degradation, the slope of the line for microdroplet slipping decreased by thermal degradation in Fig. 5(b). In interfacial property, generally, high modulus for matrix results in higher IFSS due to good 'stress transferring effect' by the rigid matrix between matrix and fiber. In the case of the ABC added EP matrix, it was found that ABC added EP matrix exhibited higher modulus than the neat EP matrix in Fig. 3.

Fig. 6 and Table 2 show the IFSS and the decrease ratio of the IFSS for different ABC weight fractions and thermal degradation times. In Fig. 6 (a) the IFSS of CF/ABC-EP composite increased to some extent as the ABC weight fraction increased up to 10 wt% whereas a steep decrease exhibited for the 20 wt% case. However, the degradation ratio of IFSS decreased continuously as the ABC weight fraction increased. Higher ABC ratio, the lower degradation ratio. As shown in the initial photos, both the neat and 10 wt% ABC added microdroplets were fractured at

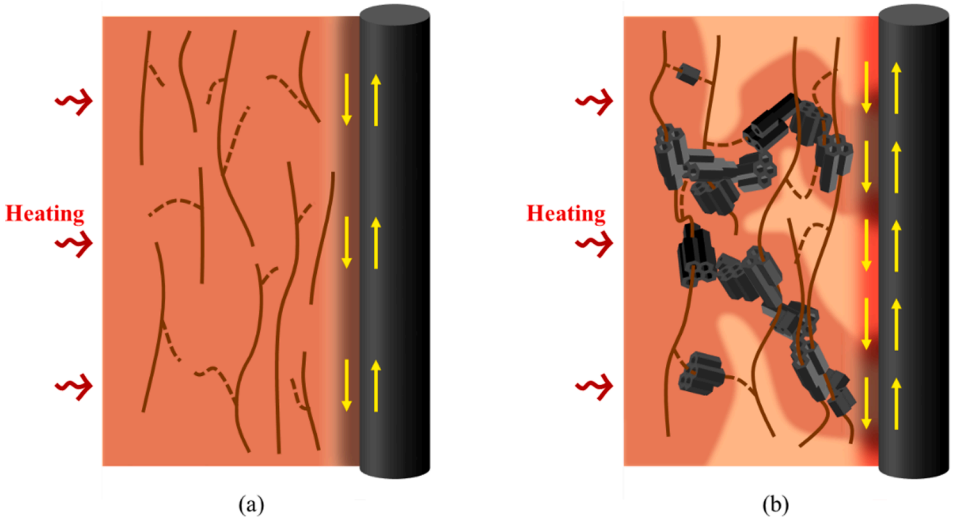

Fig. 9. Schematic plot of the interface between CF and EP: (a) neat; and (b) ABC added.

the tip of microdroplet and pulled out of CF due to reasonable rigid matrix with higher IFSS. After 30 days of thermal degradation, however, the microdroplets exhibited pulled out at neat specimen due to lower IFSS while the ABC 10 wt% added specimen was still fractured at the tip.

In Fig. 6(b), the difference in the IFSS was compared with different ABC weight fractions. The 5 and 10 wt% ABC added specimens exhibited higher IFSS than the neat specimen. The 10 wt% ABC added specimen exhibited the highest IFSS than other specimens for both the initial and 30 days thermal degradation. In case of 20 wt% ABC added specimen, the IFSS was lower than the neat specimen at the initial time. After 30 days, however, the IFSS of 20 wt% ABC added specimen was still rather higher than the neat specimen.

3.3. ILSS of CF/ABC-EP composites with different ABC weight fractions

Fig. 7 shows the ILSS for CF/ABC-EP composites with different ABC weight fractions *versus* thermal degradation time. In Fig. 8(a) at the initial time, the ILSS of the CF/ABC-EP composite increased slightly as the ABC weight fraction increased up to 10 wt%. This might be attributed to the ABC being impregnated among the CFs with a resulting increase in resistance to shear force. As the ABC weight fraction increased to 20 wt%, there was a dramatic decrease in ILSS, likely associated with the decrease in tensile and bending strength shown in Fig. 4. The error bar of ILSS increased as the ABC weight fraction increased. Especially 20 wt% ABC added CF/EP composite exhibited the largest error bar than other conditions. Because the viscosity of ABC-EP matrix increased and ABC was not dispersed well in EP matrix, the ILSS of CF/ABC-EP composite decreased gradually as the thermal degradation times increased. Fig. 8(b) shows the ILSS difference of ABC added specimens with neat specimen. The 5 wt% ABC added specimen exhibited the point of inflection after 10th days of thermal degradation. In case of 5 wt% ABC added specimen, ABC was burned out after 10 days and the ILSS decreased more quickly. In other specimens, however, the ILSS difference with neat specimen increased gradually with elapsing time.

Fig. 8 shows the photos of the interface between CF and EP with ABC addition and thermal degradation. In Fig. 8(a) and (b), the gap between CF and EP increased with thermal degradation at 120 °C for 10 days. In Fig. 8(c), however, the gap between CF and EP was less existed with the ABC addition in EP resin. Since CF and EP were contacted more closely than neat specimen, it was proved that the interfacial property of ABC added specimen was enhanced than neat specimens. Fig. 8(d) exhibited detached CF and EP due to thermal degradation and thus decreased

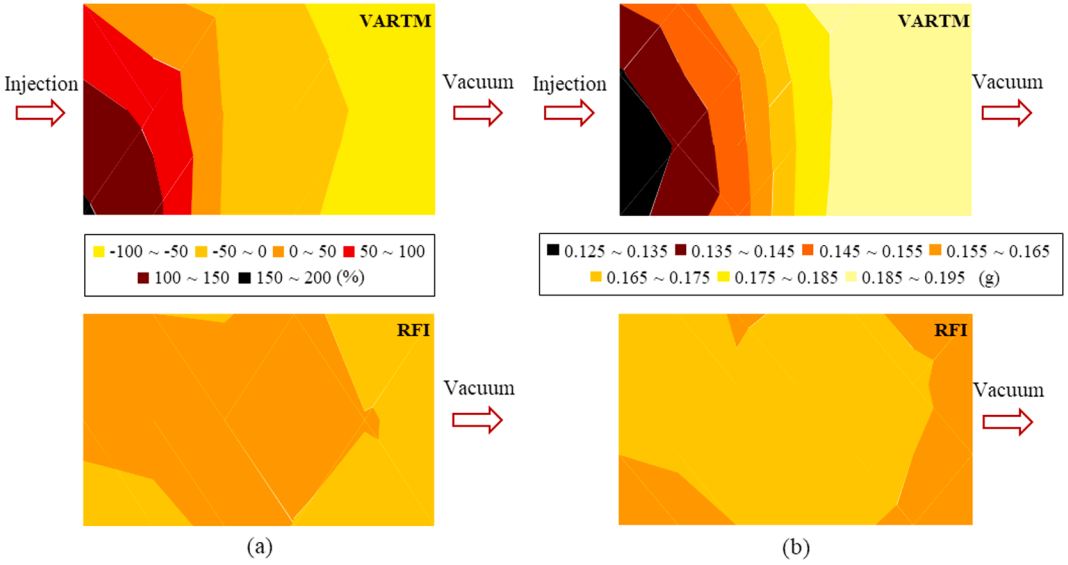

Fig. 10. 2-D mapping of CF/BC-EP composites with VARTM and RFI processes: (a) ER mapping; and (b) weight mapping.

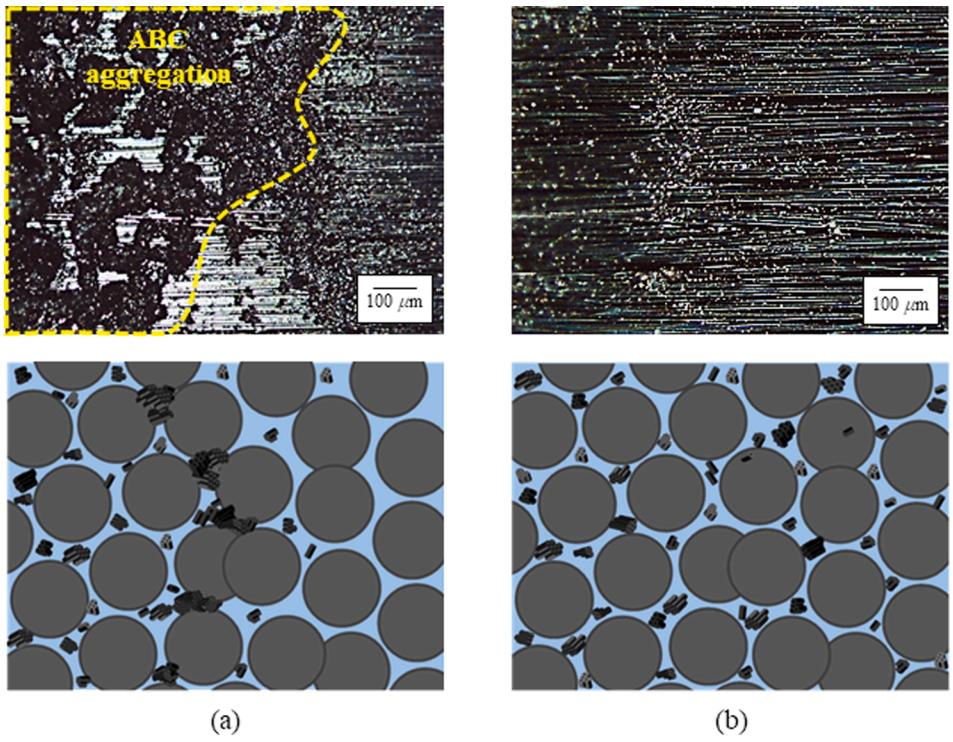

Fig. 11. Schematic plots of manufacturing process of CF/BC added EP composites: (a) VARTM; and (b) RFI.

interfacial property. Comparing with figures (b) and (d), the gap between CF and EP decreased as the ABC was added in EP resin. It was proved that the interfacial property and thermal resistivity were improved with ABC addition.

Fig. 9 shows the schematic plot of the interface between CF and ABC added EP in thermal degradation. In case of neat specimen in Fig. 9(a), the thermal energy was dissipated to whole EP matrix directly. The mechanical property of EP matrix deteriorated and micro-cracks could occur due to brittleness after thermal degradation. Interfacial property between CF and neat EP also was reduced because of entirely degraded EP matrix. In Fig. 9(b) case of ABC added specimen, the applied heat could pass though the conductive ABC easily. It can be since ABC exhibited higher thermal conductivity than neat EP. The EP matrix around the conductive ABC was thermally degraded and thus dissipated the inside heat well. It could be considered that interfacial property between CF and ABC-EP decreased less than neat EP and EP specimen after thermal degradation.

3.4. 2D-ER variation ratio mapping of CF/ABC-EP composite with different manufacturing processes

Fig. 10 shows a 2D-ER ratio and weight variation mapping for CF/ABC-EP composites manufactured using the different manufacturing processes to demonstrate the comparative ABC dispersion. As shown in Fig. 10(a), in manufactured specimen using RTM process, the injection side in the specimen exhibited a larger ER variation than the vacuum side. Furthermore, the color of the ER mapping injection side was changed more distinctly adjacent to the injection side than it did near the vacuum side. This might be attributed to the fact that during the VARTM process, the ABC particles were filtered out by the CF fabric and the ABC was not well dispersed. However, as shown in 2D-ER mapping of manufactured specimen using RFI, there was a much smaller change in color over the whole area. In the RFI process, the ABC particles were more well dispersed and the whole specimen exhibited a more stable ER than for the specimen manufactured using VARTM. In the case of Fig. 10 (b), the weight variation mapping of specimens exhibited the same trend

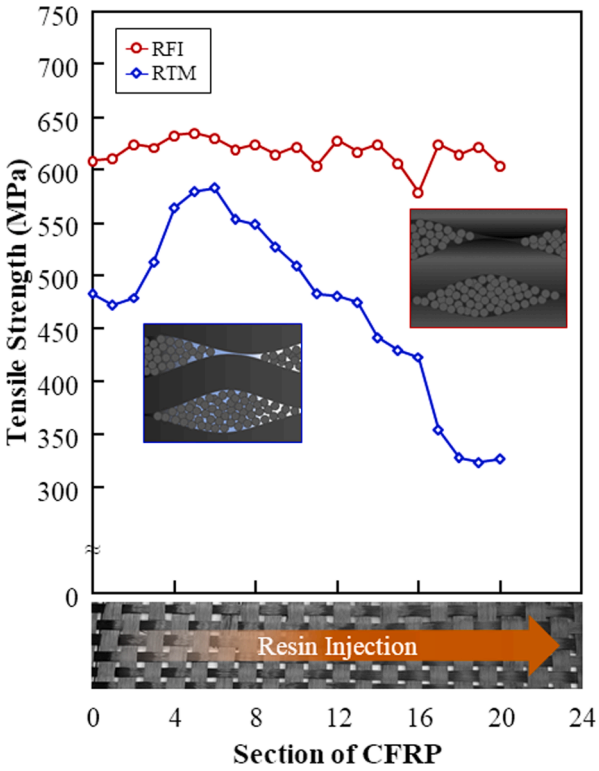

Fig. 12. Tensile strength of CF/BC added EP composite with different manufacturing methods.

with ER variation ratio mapping. In VARTM specimen, the weight increased gradually to close at the injection side and the black color exhibited. In RFI process, however, the weight of specimens was more homogeneous than VARTM specimens.

Fig. 11 exhibits the schematic plots of ABC-EP resin impregnation

with different manufacturing processes. As shown in Fig. 11(a) (VARTM process), the ABC was filtered out by CFs and the most of ABC were located in the front side. The EP resin was impregnated fully to CF fabric in length of time although the impregnation time was delayed with the ABC addition. As shown in Fig. 11(b) (RFI process), the ABC was dispersed well than VARTM process because the ABC was pre-dispersed in EP b-stage film.

Fig. 12 exhibited the tensile strength of CF/ABC-EP composite with different manufacturing methods. In case of CF/ABC-EP composites manufactured using RFI process, tensile strengths were stable in the entire sections. On the other hand, in case of using RTM process, the CF/ABC-EP composite exhibited lower tensile strengths than using RFI process. It might be due to the different dispersion states of ABC in CF/EP composite. In RTM process, the ABC was filtered by CF fabric and the CF/EP composite exhibited low tensile strength to approximately 480 MPa at resin injection section. The tensile strength increased vertically to 580 MPa up to section 3 and then decreased continuously. Tensile strength by RTM was lower than those of CF/ABC-EP composite by RFI process. In these sections, the residue ABC was observed in CF fabric, whereas the ABC was not existed than using RFI process. At over section 6, tensile strength decreased significantly to 310 MPa and it occurred because EP resin was not impregnated fully by filtered ABC.

4. Conclusions

The research motivation was to use charcoal as a reinforcement in composite materials to achieve improved mechanical and thermal properties. It was confirmed that the thermal property of EP matrix was improved as the ABC weight fraction increased. The mechanical properties of ABC-EP matrix composites increased as the ABC weight fraction increased to 10 wt%. As ABC was contained over 10 wt%, however, the mechanical properties decreased seriously. It was because increased viscosity of the ABC-EP and the poor dispersion of ABC. Interfacial properties increased as the ABC weight fraction increased up to 10 wt%. After then, both IFSS and ILSS decreased steeply due to the decrease in mechanical properties of ABC-EP matrix. From this result, the 10 wt% ABC added CF/EP composite was set as an optimized condition for most of mechanical and interfacial properties. The specimen manufactured by the RFI process exhibited more stable and reliable tensile strength than a specimen manufactured by the VARTM process. The RFI process could be considered as the recommendable method for particle reinforced epoxy composites than VARTM process in terms of the uniform ER mapping results.

CRediT authorship contribution statement

Jong-Hyun Kim: Writing – original draft, Data curation, Writing – review & editing, Visualization, Formal analysis. **Pyeong-Su Shin:** Writing – review & editing. **Dong-Jun Kwon:** Formal analysis, Visualization, Data curation. **K. Lawrence DeVries:** Writing – review & editing. **Joung-Man Park:** Formal analysis, Writing – review & editing, Visualization, Supervision. **:** .

Declaration of Competing Interest

The authors declare that they have no known competing financial interests or personal relationships that could have appeared to influence the work reported in this paper.

Acknowledgements

This research was supported by Basic Science Research Program through the National Research Foundation of Korea(NRF) funded by the Ministry of Education(No. 2016R1D1A1B01012620), 2016-2022.

References

[1] Das O, Bhattacharyya D, Sarmah AK. Sustainable eco–composites obtained from waste derived biochar: a consideration in performance properties, production costs, and environmental impact. J. Clean. Prod. 2016;129:159–68. https://doi.org/10.1016/j.jclepro.2016.04.088.
[2] Srinivasan P, Sarmah AK, Smernik R, Das O, Farid M, Gao W. A feasibility study of agricultural and sewage biomass as biochar, bioenergy and biocomposite feedstock: Production, characterization and potential applications. Sci. Total Environ. 2015;512:495–505. https://doi.org/10.1016/j.scitotenv.2015.01.068.
[3] Dahal RK, Acharya B, Saha G, Bissessur R, Dutta A, Farooque A. Biochar as a filler in glassfiber reinforced composites: Experimental study of thermal and mechanical properties. Compos. B. Eng. 2019;175:107169. https://doi.org/10.1016/j.compositesb:2019.107169.
[4] Li S, Huang A, Chen YJ, Li D, Turng LS. Highly filled biochar/ultra-high molecular weight polyethylene/linear low density polyethylene composites for high-performance electromagnetic interference shielding. Compos. B. Eng. 2018;153:277–84. https://doi.org/10.1016/j.compositesb.2018.07.049.
[5] Marris E. Putting the carbon back: black is the new green. Nature 2006;442(7103):624–6. https://doi.org/10.1038/442624a.
[6] Samantrai SP, Raghavendra G, Acharya SK. Effect of carbonization temperature and fibre content on the abrasive wear of rice husk char reinforced epoxy composite. Proc. Inst. Mech. Eng. Part J. 2014;228(4):463–9. https://doi.org/10.1177/1350650113516435.
[7] Behazin E, Misra M, Mohanty AK. Sustainable biocarbon from pyrolyzed perennial grasses and their effects on impact modified polypropylene biocomposites. Compos. B. Eng. 2017;118:116–24. https://doi.org/10.1016/j.compositesb.2017.03.003.
[8] Osman MA, Atallah A. Interparticle and particle–matrix interactions in polyethylene reinforcement and viscoelasticity. Polymer. 2005;46(22):9476–88. https://doi.org/10.1016/j.polymer.2005.07.030.
[9] Kargarzadeh H, Huang J, Lin N, Ahmad I, Mariano M, Dufresne A, et al. Recent developments in nanocellulose-based biodegradable polymers, thermoplastic polymers, and porous nanocomposites. Prog. Polym. Sci. 2018;87:197–227. https://doi.org/10.1016/j.progpolymsci.2018.07.008.
[10] Das O, Sarmah AK, Bhattacharyya D. Nanoindentation assisted analysis of biochar added biocomposites. Compos. B. Eng. 2016;91:219–27. https://doi.org/10.1016/j.compositesb.2016.01.057.
[11] Zhu S, Guo Y, Chen Y, Su N, Zhang K, Liu S. Effect of the incorporation of nano-bamboo charcoal on mechanical porperties and thermal behavior of bamboo-plastic composites. Bioresour. Technol. 2016;11:2684–97. https://doi.org/10.15376/biores.11.1.2684-2697.
[12] Jia W, Wang J, Ma L, Ren S, Yang S. Mechanical properties and thermal stability of porous polyimide/hollow mesoporous silica nanoparticles composite films prepared by using polystyrene microspheres as the pore-forming template. J. Appl. Polym Sci. 2020;137(23):48792. https://doi.org/10.1002/app.v137.2310.1002/app.48792.
[13] Tareq MS, Zainuddin S, Woodside E, Syed F. Investigation of the flexural and thermomechanical properties of nanoclay/graphene reinforced carbon fiber epoxy composites. J. Mater. Res. 2019;34(21):3678–87. https://doi.org/10.1557/jmr.2019.302.
[14] Caldwell KB, Berg JC. Self-assembly of nanoparticle-rich interphases in fiber reinforced polymeric composites using migrating agents. J. Adhes. Sci. Technol. 2018;32:1925–33. https://doi.org/10.1557/jmr.2019.302 10(1080/01694243), pp. 1453230, 2018.
[15] Kwon D-J, Shin P-S, Kim J-H, Baek Y-M, Park H-S, DeVries KL, et al. Interfacial properties and thermal aging of glass fiber/epoxy composites reinforced with SiC and SiO_2 nanoparticles. Compos. B. Eng. 2017;130:46–53. https://doi.org/10.1016/j.compositesb:2017.07.045.
[16] Van Velthem P, Ballout W, Daoust D, Sclavons M, Cordenier F, Henry E, et al. Influence of thermoplastic diffusion on morphology gradient and on delamination toughness of RTM-manufactured composites. Compos. Part. A. Appl. Sci. Manuf. 2015;72:175–83. https://doi.org/10.1016/j.compositesa:2015.02.012.
[17] Dai H, Thostenson ET. Scalable and multifunctional carbon nanotube-based textile as distributed sensors for flow and cure monitoring. Carbon. 2020;164:28–41. https://doi.org/10.1016/j.carbon.2020.02.079.
[18] Gnidakouong JRN, Roh HD, Kim JH, Park YB. In situ assessment of carbon nanotube flow and filtration monitoring through glass fabric using electrical resistance measurement. Compos. Part. A. Appl. Sci. Manuf. 2016;90:137–46. https://doi.org/10.1016/j.compositesa.2016.07.005.
[19] Garschke C, Weimer C, Parlevliet PP, Fox BL. Out-of-autoclave cure cycle study of a resin film infusion process using in situ process monitoring. Compos. Part. A. Appl. Sci. Manuf. 2012;43(6):935–44. https://doi.org/10.1016/j.compositesa:2012.01.003.
[20] Ma X, Yang Z, Gu Y, Li Y, Li M, Zhang D, et al. Manufacture and characterization of carbon fiber composite stiffened skin by resin film infusion/prepreg co-curing process. J. Reinf. Plast. Compos. 2014;33(17):1559–73. https://doi.org/10.1177/0731684414543213.
[21] Wang B, Duan Y, Xin Z, Yao X, Abliz D, Ziegmann G. Fabrication of an enriched graphene surface protection of carbon fiber/epoxy composites for lightning strike via a percolating-assisted resin film infusion method. Compos. Sci. Technol. 2018;158:51–60. https://doi.org/10.1016/j.compscitech.2018.01.047.
[22] Marriam I, Xu F, Tebyetekerwa M, Gao Y, Liu W, Liu X, et al. Synergistic effect of CNT films impregnated with CNT modified epoxy solution towards boosted interfacial bonding and functional properties of the composites. Compos. Part. A.

Appl. Sci. Manuf. 2018;110:1–10. https://doi.org/10.1016/j.compositesa:2018.04.011.
[23] Anand A, Harshe R, Joshi M. Resin film infusion: toward structural composites with nanofillers. J. Appl. Polym. Sci. 2013;129(3):1618–24. https://doi.org/10.1002/app.38855.
[24] Yourdkhani M, Liu W, Baril-Gosselin S, Robitaille F, Hubert P. Carbon nanotube-reinforced carbon fibre-epoxy composites manufactured by resin film infusion. Compos. Sci. Technol. 2018;166:169–75. https://doi.org/10.1016/j.compscitech.2018.01.006.
[25] Tan Yi, Shao Z-B, Yu L-X, Xu Y-J, Rao W-H, Chen Li, et al. Polyethyleneimine modified ammonium polyphosphate toward polyamine-hardener for epoxy resin: Thermal stability, flame retardance and smoke suppression. Polym. Degrad. Stab. 2016;131:62–70. https://doi.org/10.1016/j.polymdegradstab.2016.07.004.
[26] Kim J-H, Kwon D-J, Shin P-S, Baek Y-M, Park H-S, Lawrence DeVries K, et al. New evaluation of interfacial properties and damage sensing in CFRC by VARTM using 3D ER mapping. Compos. B. Eng. 2018;155:178–86. https://doi.org/10.1016/j.compositesb:2018.08.010.
[27] Kim JH, Kwon DJ, Shin PS, Baek YM, Park HS, DeVries KL, et al. The evaluation of the interfacial and flame retardant properties of glass fiber/unsaturated polyester composites with ammonium dihydrogen phosphate. Compos. B. Eng. 2016;167:221–30. https://doi.org/10.1016/j.compositesb.2018.12.032.
[28] Wang Z-J, Kwon D-J, Choi J-Y, Shin P-S, Yi J-W, Byun J-H, et al. Inherent and interfacial evaluations of carbon nanotubes/epoxy composites and single carbon fiber at different temperatures. Compos. B Eng. 2016;91:111–8. https://doi.org/10.1016/j.compositesb:2015.12.036.
[29] Das O, Bhattacharyya D, Hui D, Lau KT. Mechanical and flammability characterisations of biochar/polypropylene biocomposites. Compos. B. Eng. 2016;106:120–8. https://doi.org/10.1016/j.compositesb.2016.09.020.
[30] Bowlby LK, Saha GS, Afzal MT. Flexural strength behavior in pultruded GFRP composites reinforced with high specific-surface-area biochar particles synthesized via microwave pyrolysis. Compos A Appl Sci Manuf 2018;110:190–6. https://doi.org/10.1016/j.compositesa.2018.05.003.